Taylor & Francis
Taylor & Francis Group

FIBER AND INTEGRATED OPTICS

Fiber and Integrated Optics

ISSN: (Print) (Online) Journal homepage: https://www.tandfonline.com/loi/ufio20

Design of Ultra-High Sensitivity Slot Micro-ring Resonator Acoustic Sensor

Xiaoxia Chu, Jiangong Cui, Min Zhu, Rongyu Zhao, Wendong Zhang, Guojun Zhang, Renxin Wang, Yuhua Yang & Yongfeng Ren

To cite this article: Xiaoxia Chu, Jiangong Cui, Min Zhu, Rongyu Zhao, Wendong Zhang, Guojun Zhang, Renxin Wang, Yuhua Yang & Yongfeng Ren (2022): Design of Ultra-High Sensitivity Slot Micro-ring Resonator Acoustic Sensor, Fiber and Integrated Optics, DOI: 10.1080/01468030.2022.2145529

To link to this article: https://doi.org/10.1080/01468030.2022.2145529

Published online: 11 Nov 2022.

FIBER AND INTEGRATED OPTICS
https://doi.org/10.1080/01468030.2022.2145529

Taylor & Francis
Taylor & Francis Group

Design of Ultra-High Sensitivity Slot Micro-ring Resonator Acoustic Sensor

Xiaoxia Chu, Jiangong Cui, Min Zhu, Rongyu Zhao, Wendong Zhang, Guojun Zhang, Renxin Wang, Yuhua Yang, and Yongfeng Ren

State Key Laboratory of Dynamic Measurement Technology, North University of China, Taiyuan, Shanxi, China

ABSTRACT

A slot microring resonator acoustic sensor (MRAS) using the PDMS package was proposed to achieve ultra-high sensitivity acoustic detection. The acoustic detection principle of the sensor is analyzed theoretically, the structural parameters are optimized and the performance of the sensor is verified by simulation. The simulation results show that the proposed slot MRAS has a high-quality factor of 1.49×10^6, the sensitivity of the sensor by intensity detection method is up to 3872 mV/kPa, and the 3 dB bandwidth is 210 MHz. The sensor designed in this paper has the advantages of ultra-high sensitivity and wide bandwidth range, which has important value in the field of acoustic detection.

ARTICLE HISTORY
Received 19 August 2022
Accepted 5 November 2022

KEYWORDS
Acoustic detection; PDMS; slot micro-ring resonator; ultra-high sensitivity

1 Introduction

Acoustic detection plays an irreplaceable role in nondestructive testing [1], acoustic microscopy [2], medical imaging [3, 4] and other fields. Acoustic sensors can be divided into two types. One is electric-acoustic sensor [5–7]. However, such hydrophones have certain defects, such as poor anti-electromagnetic interference ability, narrow response band, low sensitivity, especially poor reuse ability; The other is the photo-acoustic sensor [8–11], which has the favorable advantages of strong electromagnetic interference resistance, high sensitivity, large bandwidth range, small volume and easy integration Compared with the traditional electric-acoustic sensor. At present, the pure optical acoustic signal testing technology instead of piezoelectric detection is the development demand of the future. However, the acoustic signal testing technology based on Fabry–Perot interferometer (FPI) [8], polymer film interference [9], fiber or grating FPI [10, 11] mostly relies on the strain variable of mechanical deformation to realize the sensing of acoustic signal, which results in self-resonance and frequency narrowing. Therefore, it is the development trend of military application field to explore a new method

CONTACT Yongfeng Ren renyongfeng@nuc.edu.cn State Key Laboratory of Dynamic Measurement Technology, North University of China, Taiyuan 030051, China

of sound signal testing without diaphragm, all solid state and pure optics, and to achieve ultra-wide band and high-sensitivity sound signal testing.

In recent years, pure optical micro-ring ultrasonic sensors without diaphragm have been widely studied. For instance, Ling T, and so on, from The University of Michigan [12–14] conducted continuous and in-depth research on polymer micro-ring ultrasonic sensors. Literature [14] proposed a micro-ring ultrasonic sensor with a radius of 30 μm, which has a quality factor of 3×10^5. The sensor achieves a sensitivity of 36.3 mV/kPa and a 3 dB bandwidth of 350 MHz. However, polymers typically have a refractive index of about 1.5, which means that a low refractive index difference can limit device performance when the device is relatively small. In 2021, Wouter J. Westerveld, etc., [15] designed and prepared a silicon waveguide ultrasonic sensor. The sensitivity of a micro-ring resonator with a radius of 20 um is 2.5 mV/kPa under the action of ultrasonic signals in the range of 3–30 MHz. The silicon micro-ring ultrasonic detector has the advantages of CMOS compatibility, small size and high-quality factor, which are important factors in determining the sensitivity of ultrasonic detector. However, the sensitivity of this ultrasonic sensor is still very low. The slit waveguide structure in the silicon micro-ring resonator can improve the sensitivity and have a higher Q factor. In order to make the ultrasonic field have a strong interaction with the optical field, the ultrasonic detector based on the slit optical micro-cavity generally adopts polymers with lower Young's modulus as the upper cladding of the micro-ring resonator [16, 17]. In 2017, a kind of SU8 polymer micro-ring ultrasonic detector was proposed [16], with a theoretical Q value as high as 8.34×10^8, and its sensitivity is 165.7 times that of the polymer ultrasonic sensor.

In order to obtain higher acoustic detection sensitivity of slit waveguide, a new slot PDMS polymer (low Young's modulus and large Poisson's ratio, compared with other polymers) micro-ring ultrasonic sensor is proposed in this paper, which has not been mentioned in previous studies. The size of the structure is optimized through simulation to maximize the Q value of the device. The ultrasonic detection characteristics of the proposed sensor are studied by COMSOL software. The results show that the ultrasonic sensor proposed in this paper has ultra-high sensitivity and wide frequency range compared with the previously studied acoustic sensing structure, which has practical reference significance in the field of acoustic detection.

2 Principle

2.1 Principle of slot MRAS

The slot micro-ring resonator (MRAS) structure as shown in Figure 1(a). The under cladding is silicon dioxide, the core layer consists of a straight waveguides and two concentric circular waveguide, dozens of nanometer gap

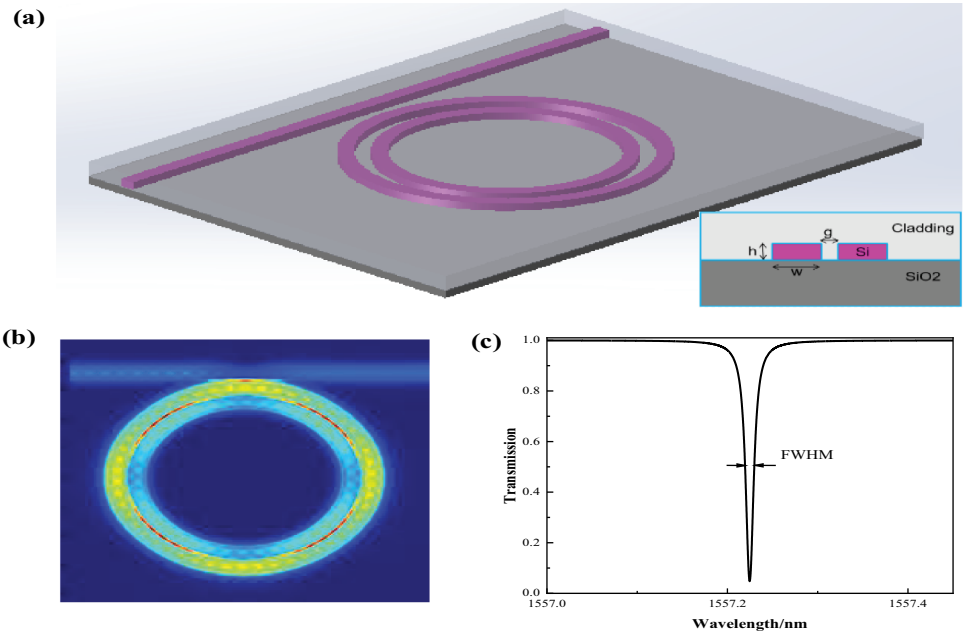

Figure 1. Schematic of ultrasonic sensor based on slot MRR: (a)3D Structure view of slot MRR and Cross section of Slot Wave-guide. (b)Optic field distribution in resonant state. (c)Transmission of slot MRR.

between each two circular waveguides form a micro slot, the upper cladding is polymer that also acts as a medium of ultrasonic sensor. The illustration shows the cross section of the micro slot. In the process of light transmission in the straight waveguide, part of the light enters the ring waveguide on account of evanescent field effect, the light field in the micro-ring interferes with the light field in the straight waveguide after one round of transmission, and the light meeting the resonance conditions will enter the micro-ring and generate resonance enhancement effect. Resonance conditions can be expressed as [17]

$$m\lambda = n_{eff}L \tag{1}$$

Here, m represents the resonant order, λ represents the resonant wavelength, n_{eff} represents the effective refractive index, L represents the circumference of the micro-ring. A strong light field will be formed in the slot micro-ring by repeated interference. The light field distribution of the slot MRR when it reaches the resonance state is shown in Figure 1(b). The transmission spectrum of the output port is shown in Figure 1(c), which can be calculated by the following formula:

$$T = \frac{a^2 + t^2 - 2at\cos\varphi}{1 + a^2t^2 - 2at\cos\varphi} \tag{2}$$

Where a represents the loss of light transmitted in the slot micro-ring waveguide for one round, it be expressed as a = exp(-πRα_R), α_R represents the loss factor, t represents for transmission coefficient, φ represents the phase change of the light after one week of transmission in the grooved micro-ring waveguide. When the transmission spectrum is the minimum value, it means that the slot MRR has reached the resonance state, and the corresponding wavelength is the resonant wavelength. We can determine the information of the ultrasonic signal by measuring the drift of the resonant wavelength in the transmission spectrum in the actual ultrasonic signal sensing.

The performance of slot MRAS can be measured by its quality factor Q. It can be expressed as [18]

$$Q = \frac{\pi L n_g \sqrt{ta}}{\lambda(1-ta)} \tag{3}$$

Where $n_g = n_{eff} - \lambda_0 \frac{dn_{eff}}{d\lambda}$ represents the group index, which takes into account the dispersion of the waveguide. It can be seen from the above equation that the Q value of the slot MRAS is proportional to the circumference of the micro-ring.

2.2 Principle of ultrasonic detection

According to the optical waveguide mode theory, the evanescent field distribution state of the waveguide will be changed when the refractive index of cladding layer on the MRAS changes, which change the effective refractive index of the device and make the resonant wavelength shift. When the slot MRAS is used as an acoustic sensor, the upper cladding plays the role of sensing medium and produces strain under the action of ultrasonic signal, which changes the effective refractive index of the slot waveguide through deformation and elastic-optical effect. The relationship between strain and sound pressure can be expressed in Equation (4) [19] and the relationship between refractive index and strain can be expressed in Equation (5) [20].

$$\varepsilon = -\frac{(1+\nu)(1-2\nu)P}{E} \tag{4}$$

$$\frac{\Delta n}{n_0} = -\frac{n_0^2 \varepsilon}{2}[p_{12} - \nu(p_{11} + p_{12})] \tag{5}$$

Where, ν represents the Poisson's ratio of the material, E represents the Young's Modulus of the material, P_{11} and P_{12} represent the first and second stress optical coefficients of the material respectively, P represents the ultrasonic pressure, and n_0 represents the refractive index of the material without the action of sound pressure. It can be seen from Eq. (4) and Eq. (5) that the

Table 1. Properties of several polymers.

Materials	Refractive index	Young's modulus	Poisson's ratio
SU8	1.57	4.02 GPa	0.22
PMMA	1.46	3 GPa	0.4
PS	1.58	0.3 GPa	0.33
PDMS	1.406	0.75 MPa	0.49

strain relate to the Poisson's ratio and Young's modulus of the material. The larger the Poisson's ratio is and the smaller the Young's modulus is, the larger the strain of the material is under the same sound pressure, leading to the larger refractive index change. Related parameters of several polymers are given in Table 1. PDMS polymers have the characteristics of low Young's modulus and large Poisson's ratio compared with other polymers. Therefore, PDMS polymer is selected as the upper cladding of slot MRR as an ultrasonic sensing medium in this paper.

3 Design and optimization of slot MRAS

Reference [21] pointed out that MRAS with high Q factor would be beneficial to improve its ultrasonic detection sensitivity, so it is necessary to optimize the design of slot MRAS to improve the sensor performance. According to the Equation (3), the Q value of the micro-ring is proportional to the effective refractive index and the circumference of the micro-ring, hence the Q value of the device can be optimized from the perspective of the effective refractive index and cavity length.

Firstly, the relationship between the effective refractive index and waveguide width in the polarization modes of TE0 and TE1 is studied, as shown in Figure 2(a), the larger the waveguide width is, the higher the effective refractive

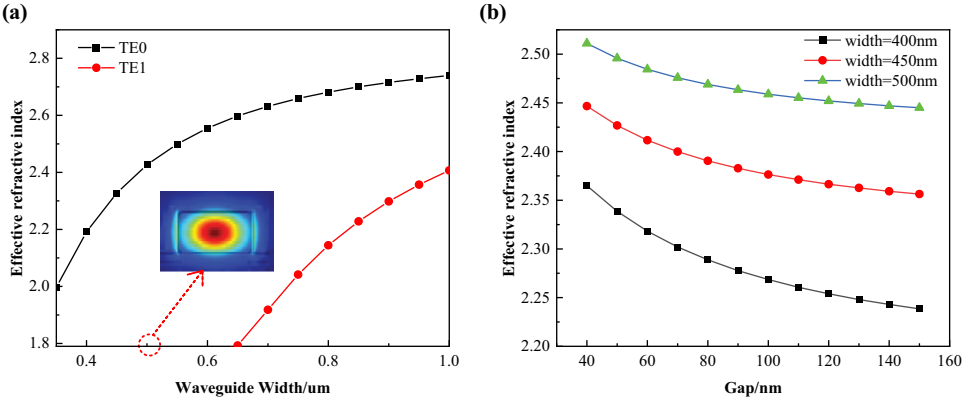

Figure 2. (a)Effective refractive index of the different order of TE modes with the waveguide width at 1550 nm wavelength. (b)Effective refractive index of the different waveguide width with the waveguide gap.

index is. Only the fundamental mode exists in the waveguide when the waveguide width is between 0.35 μm and 0.65 μm, the inset shows the fundamental mode distribution when the width of the waveguide is 0.5 μm. There are higher-order modes in the waveguide when the width of the waveguide is greater than 0.65 μm. Figure 2(b) shows the relationship between effective refractive index and gap under different waveguide widths. The results show that when the waveguide width is constant, the larger the gap is, the lower the effective refractive index is; when the waveguide gap is constant, the larger the waveguide width is, the larger the effective refractive index is. Combined with the analysis results of Figure 2(a,b), in order to allow only fundamental mode transmission in the waveguide and make the effective refractive index as large as possible, a waveguide width of 0.5 μm is designed in this paper.

Figure 3 shows the light field distribution under different gap when the waveguide width is 0.5 μm. The effects of curvature and dispersion on waveguide mode and the existence of anti-propagation field are ignored in the two-dimensional simulation [22]. It can be seen from the figure that the smaller the gap, the stronger the local ability to light. However, the small gap width is not conducive to the filling of PDMS, so the gap width of 80 nm is selected in this paper.

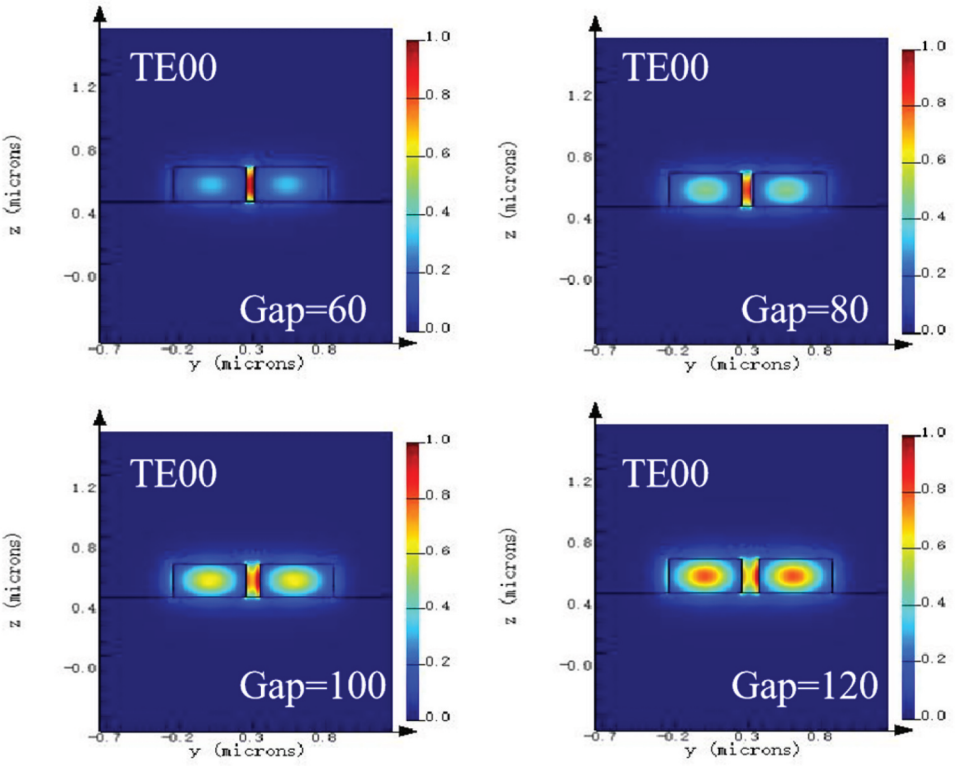

Figure 3. The electric field pattern distribution diagram with a width of 500 nm and different gaps.

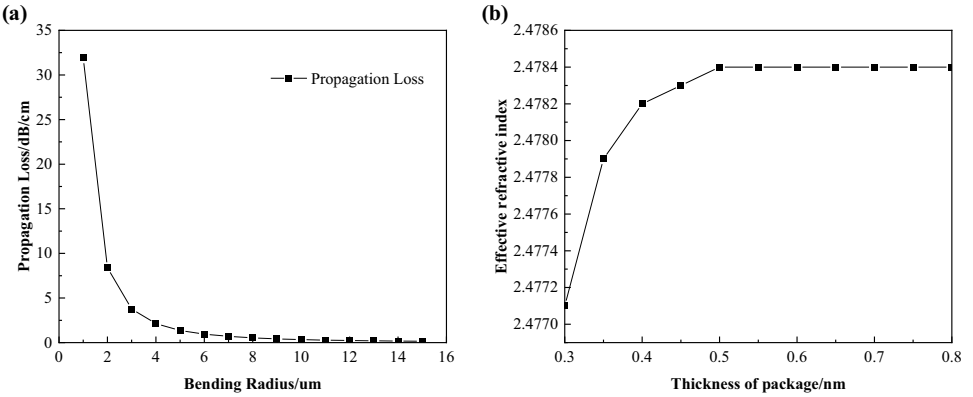

Figure 4. (a)The relationship between Bending radius and the propagation loss. (b)The relationship between Thickness of package and Effective refractive index.

Table 2. Description of structure parameters of Slot micro-ring ultrasonic sensor.

Structural parameters	Value	Description of parameters
w	500 nm	waveguide width
h	220 nm	waveguide height
g	80 nm	microring gap
R	10 μm	radius of micro-ring
G	120 μm	Coupling interval
H	0.5 μm	PDMS height

Figure 4(a) shows the relationship between the propagation loss and the bending radius of slot MRAS, it can be seen that the bending radius has a significant influence on the bending loss, and the bending loss decreases with the increase of the bending radius. When the bending radius is larger than 9 μm, the bending loss is very small and can be ignored. In order to minimize the device structure and bending loss, the micro-ring radius is designed as 10 μm in this paper. Figure 4(b) shows the relationship between the effective refractive index and the PDMS cladding thickness. The results show that the effective refractive index increases with the increase of the PDMS thickness when the PDMS thickness is less than 0.5 μm and remains almost constant when the PDMS thickness is greater than 0.5 μm. Accordingly, PDMS was selected as the upper cladding layer with a thickness of 0.5 μm to make the effective refractive index higher.

In conclusion, the structural parameters of the slot MRAS proposed in this paper are shown in Table 2. According to Eq. (3), the Q value of the sensor is as high as 1.49×10^6 theoretically.

4 Simulation results and analysis

4.1 Sensitivity analysis

COMSOL software was used to simulate the photo-acoustic coupling to verify the ultrasonic sensing performance of the proposed Slot MRAS. The photo-acoustic coupling model of the Slot MRAS is shown in Figure 5(a), the black waveform represents the applied ultrasonic signal, and the red arrow represents the input optical signal with an optical power of 1 mW and wavelength of 1.55 μm, the blue arrow indicates the output optical signal. Considering the proposed model is not suitable for 3D finite element analysis due to the large memory required and long computational time, in order to quantitatively calculate the change of the effective refractive index of slit waveguides induced by sound pressure, two-dimensional finite element simulation of the acoustic-solid interaction is carried out by COMSOL software. In the simulation, electromagnetic wave (frequency domain), pressure acoustic (frequency domain), solid mechanical models are used. The Poisson ratios of PDMS, silicon and silica were 0.49, 0.3 and 0.25, and the young's moduli were 0.75 MPa, 100 GPa and 85 GPa, respectively. A multi-physical field module is used to realize the acoustic-structure coupling. The top of the PDMS cladding is set as the boundary between sound waves and the structure. At the same time, the refractive index of the structural material in different directions (x,y,z) is set in the electromagnetic wave (frequency domain) module based on the elastic-

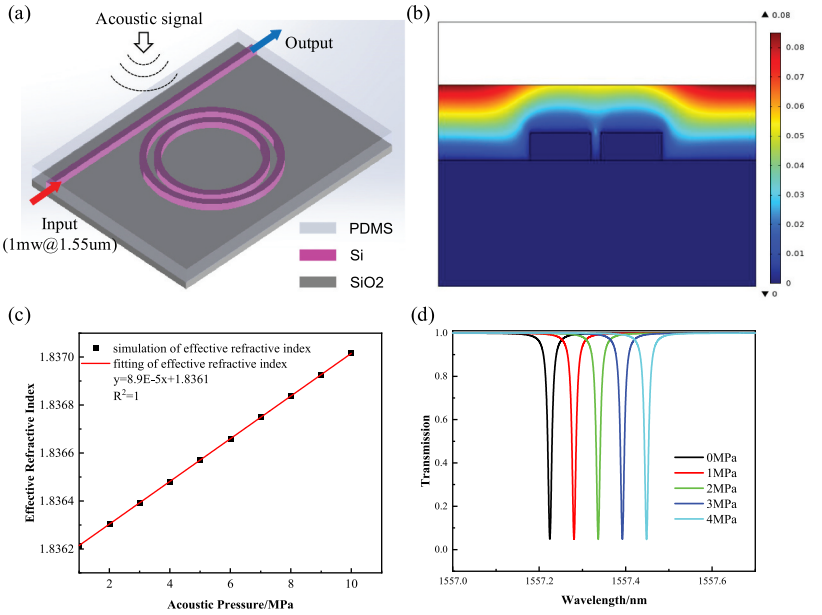

Figure 5. (a)Schematic diagram of photo-acoustic coupling model. (b)Schematic diagram of deformation. (c) the relationship between different sound pressures and the effective refractive index. (d) spectrum response curve under different sound pressure.

optical theory [23]. The silica substrate boundary is fixed and all materials are free to deform according to the stress generated by the ultrasonic wave. Use a free triangle to create the mesh and set it to super refined. The scanning range of parametric is from 1 MPa to 10 MPa with interval of 1 MPa. The structure deforms after acoustic wave is applied to the top of PDMS cladding through water and the total computation time is about 83s. Figure 5(b) shows the two-dimensional deformation distribution of the slot waveguide under the ultrasonic pressure of 1 MPa, it can be obviously seen that the deformation of the upper cladding PDMS is the largest, which will significantly change the effective refractive index of the slot waveguide. Figure 5(c) is the curve of the variation relationship between different ultrasonic pressures and effective refractive index obtained through simulation calculation under the condition of elastic-optical effect, the result indicated that the effective refractive index has a linear relationship with ultrasonic pressure after fitting, which can be expressed as

$$\frac{dn_{eff}}{dP} = 8.9 \times 10^{-5}/MPa \tag{6}$$

Figure 5(d) shows the spectral line drift curves of slot MRAS under different ultrasonic pressures. According to Eq. (1), the relationship between resonant wavelength drift and sound pressure can be expressed as

$$\frac{d\lambda}{dP} = \frac{\lambda}{n_{eff}}\frac{dn_{eff}}{dP} = 0.08nm/MPa \tag{7}$$

The results show that the resonant wavelength of the proposed sensor has a linear shift of 80 pm/MPa under the action of ultrasonic wave, which is approximately nine times as high as that in literature [16].

Ultrasonic detection can be realized by detecting light intensity changes at specific wavelengths. At this time, sensitivity is defined as the ratio of transmission intensity to ultrasonic pressure, which is expressed as

$$S = \frac{\partial T}{\partial P} = \frac{\partial T}{\partial \lambda}\frac{\partial \lambda}{\partial n_{eff}}\frac{\partial n_{eff}}{\partial P} = \frac{\lambda}{n_{eff}}\frac{\partial T}{\partial \lambda}\frac{\partial n_{eff}}{\partial P} \tag{8}$$

For high Q slot micro-ring ultrasonic sensor, the transmitted light intensity is related to the position of the resonant wavelength. The resonant wavelength shift caused by the acoustic wave causes significant changes in the transmitted light intensity due to the steep resonance curve, thus improving its sensitivity. Therefore, the sensitivity can be maximized by setting the resonant point at the wavelength with the highest slope of the transmission spectrum. According to the linear relation between output light intensity and wavelength, the acoustic pressure can be demodulated. According to Eq. (8), the sensitivity of the ultrasonic sensor proposed in this paper is as high as 3872 mV/kPa.

4.2 Frequency response analysis

Frequency response plays an important role in ultrasonic detection. The frequency response characteristics of the sensor determine the frequency range to be measured and must be kept undistorted within the allowable frequency range. The higher the frequency response of the sensor, the wider the frequency range of the signal that can be measured. Therefore, it is very important to study the frequency response of the sensor. Studies [24, 25] show that the main factor of frequency response is determined by the FP cavity effect of sound waves, which can be expressed by the following formula:

$$|P_I(k)| = \frac{2T}{kl}\sqrt{\frac{(R_0^2+1)+4R_0\cos k(1+2l_0)\sin^2(kl/2)}{1-2R_0R_1\cos 2k(1+l_0)+(R_0R_1)^2}} \tag{9}$$

Here, $P_I(k)$ represents normalized frequency response, k is acoustic wave vector, T represents pressure amplitude transmission coefficient, l is upper cladding thickness, R_0 and R_1 are amplitude reflection coefficients. The acoustic impedance of PDMS is 1.06×10^6 Kg/(sm^2), and that of silica is 1.31×10^7 Kg/(sm^2), the acoustic impedance of deionized water is 1.49×10^6 Kg/(sm^2). The frequency response curve of the Slot MRAS designed for ultrasonic detection in this paper is shown in Figure 6. The sensor has a 3 dB bandwidth of 210 MHz. The performance comparison between the sensor in this paper and the sensor previously studied is shown in Table 3. The comparison results show that the sound sensor designed in this study has the advantage of ultra-high sensitivity and wide frequency range.

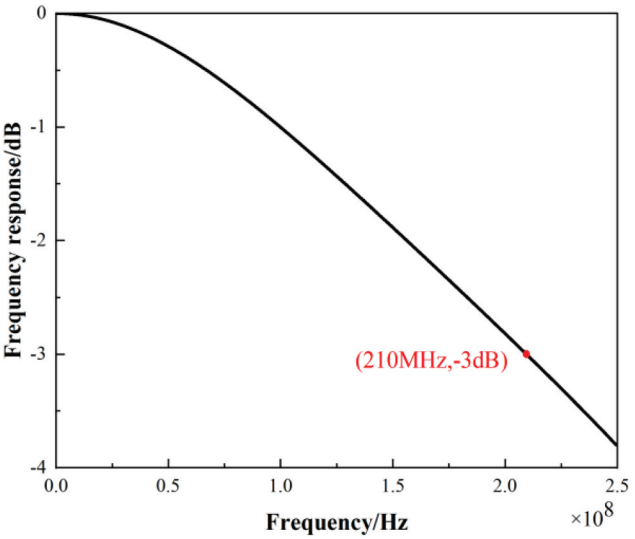

Figure 6. The frequency response of proposed Slot MRR based ultrasound detector.

Table 3. Performance comparison of micro-ring ultrasonic sensor.

Structure	dneff/dP	S(mV/kPa)	Q factor	R(μm)	3 dB bandwidth(MHz)
Polymer ring [15]	-	36.3	1×10^{7}	30	20
SU8 [16]	9×10^{-6}/MPa	66.7	8.34×10^{8}	12	540
Double ring [26]	4×10^{-6}/MPa	2453.7	1.24×10^{6}	5	150
This work	8.9×10^{-5}/MPa	3872	1.49×10^{6}	10	210

5 Conclusion

In this paper, a kind of ultra-sensitive ultrasonic sensor is proposed. The polymer PDMS with low Young's modulus is selected as the upper cladding of slot MRAS to act as the ultrasonic sensing medium. The ultrasonic detection performance of the sensor is simulated by COMSOL Multi-physics software. The sensitivity of the sensor through the intensity detection method is up to 3872 mV/KPa and bandwidth is up to 210 MHz. Compared with the previous ultrasonic sensors, the proposed ultrasonic sensor has the advantage of ultra-high sensitivity and broad band, and has good application potential in the field of ultrasonic detection.

Disclosure statement

No potential conflict of interest was reported by the author(s).

Funding

This work was supported by the National Key Research and Development Project [grant number 2019YFC0119800]; the Development Project Fundamental Research Program of Shanxi Province [grant number 202103021224203 and 20210302123027]; the National Natural Science Foundation of China [grant number 52175553]; the Fund for Shanxi "1331 Project" key Subject Construction and Innovation Special Zone Project; National Natural Science Foundation of ChinaNational Natural Science Foundation of China [52175553; the National Key Research and Development projectthe National Key Research and Development project [2019YFC0119800];Shanxi Province "1331 Project" key discipline construction plan; the Development project Fundamental Research Program of Shanxi Province [202103021224203, 20210302123027];

References

[1] M. Kersemans *et al.*, "The pulsed ultrasonic backscatter polar scan and its applications for NDT and material characterization," *Exp. Mech*, vol. 54, no. 6, pp. 1059–1071, Jul. 2014. DOI: 10.1007/s11340-013-9843-1.

[2] C. Errico *et al.*, "Ultrafast ultrasound localization microscopy for deep super-resolution vascular imaging," *Nat*, vol. 527, no. 7579, pp. 499–502, Nov. 2015. DOI: 10.1038/nature16066.

[3] X. Wang, Y. Pang, K. Geng, X. Xie, and L. V. Wang, "Noninvasive laser-induced photoacoustic tomography for structural and functional in vivo imaging of the brain," *Nat. Biotechnol*, vol. 21, no. 7, pp. 803–806, Jul. 2003. DOI: 10.1038/nbt839.

[4] C. Fei *et al.*, "Ultrahigh frequency (100MHz–300MHz) ultrasonic transducers for optical resolution medical imagining," *Sci. Rep*, vol. 6, no. 7579, pp. 28360, Jun. 2016. DOI: 10.1038/srep28360.

[5] M. Prasad, A. Aditi, and V. K. Khanna, "Development of MEMS acoustic sensor with microtunnel for high SPL measurement," *IEEE Trans. Ind. Electron*, vol. 69, no. 3, pp. 3142–3150, Mar. 2022. DOI: 10.1109/TIE.2021.3068666.

[6] B. Chen *et al.*, "AlN-based piezoelectric micromachined ultrasonic transducer for photoacoustic imaging," *Appl. Phys. Lett*, vol. 103, no. 3, pp. 031118, Jul. 2013. DOI: 10.1063/1.4816085.

[7] J. H. Han *et al.*, "Machine learning-based self-powered acoustic sensor for speaker recognition," *Nano Energy*, vol. 53, pp. 658–665, Nov. 2018. DOI: 10.1016/j.nanoen.2018.09.030.

[8] A. Wang, J. Xu, C. K.l, and X. Wang, "Miniature all-silica fiber optic pressure and acoustic sensors," *Opt. Lett*, vol. 30, no. 24, pp. 3269–3271, Dec. 2005. DOI: 10.1364/OL.30.003269.

[9] M. A. Tadayon, M. E. Baylor, and S. Ashkenazi, "Polymer waveguide Fabry-Perot resonator for high-frequency ultrasound detection," *IEEE Trans. Ultrason. Ferroelectr. Freq. Control*, vol. 61, no. 12, pp. 2132–2138, Dec. 2014. DOI: 10.1109/TUFFC.2014.006505.

[10] J. Ma *et al.*, "Fiber-optic Fabry-Perot acoustic sensor with multilayer graphene diaphragm," *IEEE Photonics Technol. Lett*, vol. 25, no. 10, pp. 932–935, May. 2013. DOI: 10.1109/LPT.2013.2256343.

[11] H. Tsuda, "Ultrasound and damage detection in CFRP using fiber Bragg grating sensors," *Compos. Sci. Technol*, vol. 66, no. 5, pp. 676–683, May. 2006. DOI: 10.1016/j.compscitech.2005.07.043.

[12] C. Y. Chao, W. Fung, and L. J. Guo, "Polymer microring resonators for biochemical sensing applications," *IEEE J. Sel. Top. Quantum Electron*, vol. 12, no. 1, pp. 134–142, Jan. 2006. DOI: 10.1109/JSTQE.2005.862945.

[13] C. Zhang, S. L. Chen, T. Ling, and L. J. Guo, "Review of imprinted polymer microrings as ultrasound detectors: design,fabrication, and characterization," *IEEE Sens. J*, vol. 15, no. 6, pp. 3241–3248, Jun. 2015. DOI: 10.1109/JSEN.2015.2421519.

[14] T. Ling, S. L. Chen, and L. J. Guo, "High-sensitivity and wide-directivity ultrasound detection using high Q polymer microring resonators," *Appl. Phys. Lett*, vol. 98, no. 20, pp. 204103, May. 2011. DOI: 10.1063/1.3589971.

[15] W. J. Westerveld *et al.*, "Sensitive, small, broadband and scalable optomechanical ultrasound sensor in silicon photonics," *Nat. Photonics*, vol. 15, no. 5, pp. 341–345, May. 2021. DOI: 10.1038/s41566-021-00776-0.

[16] S. L. Zhang, J. Chen, and S. L. He, "Novel ultrasound detector based on small slot micro-ring resonator with ultrahigh Q factor," *Opt. Commun*, vol. 382, pp. 113–118, Jan. 2017. DOI: 10.1016/j.optcom.2016.07.082.

[17] B. Su, C. Wang, Q. Kan, and H. Chen, "Compact silicon-on-insulator dual-microring resonator optimized for sensing," *J. Lightwave Technol*, vol. 29, no. 10, pp. 1535–1541, May. 2011. DOI: 10.1109/JLT.2011.2138678.

[18] W. Bogaerts *et al.*, "Silicon microring resonators," *Laser Photonics Rev*, vol. 6, no. 1, pp. 47–73, Jan. 2012. DOI: 10.1002/lpor.201100017.

[19] C. Y. Chao, S. Ashkenazi, S. W. Huang, M. O'Donnell, and L. J. Guo, "High-frequency ultrasound sensors using polymer microring resonators," *IEEE Trans. Ultrason.*

Ferroelectr. Freq. Control, vol. 54, no. 5, pp. 957–965, May. 2007. DOI: 10.1109/TUFFC.2007.341.

[20] F. Ay, A. Kocabas, C. Kocabas, A. Aydinli, and S. Agan, "Prism coupling technique investigation of elasto-optical properties of thin polymer films," *J. Appl. Phys*, vol. 96, no. 12, pp. 7147–7153, Dec. 2004. DOI: 10.1063/1.1812823.

[21] H. Li, B. Q. Dong, Z. Zhang, H. F. Zhang, and C. Sun, "H.F. Zhang and C. Sun, "A transparent broadband ultrasonic detector based on an optical micro-ring resonator for photoacoustic microscopy," *Sci. Rep*, vol. 4, no. 1, pp. 4496, Mar. 2016. DOI: 10.1038/srep04496.

[22] G. Brunetti, F. Dell' Olio, D. Conteduca, M. N. Armenise, and C. Ciminelli, "Comprehensive mathematical modelling of ultra-high Q grating-assisted ring resonators," *J. Opt*, vol. 22, no. 3, pp. 035802, Mar. 2020. DOI: 10.1088/2040-8986/ab71eb.

[23] K. Okamoto, *Fundamentals of Optical Waveguides*. San Diego, CA: Academic, 2000, pp. 265.

[24] Z. Xie *et al*., "Pure optical photo-acoustic microscopy," *Opt. Express*, vol. 19, no. 10, pp.9027934, 2011. DOI: 10.1364/OE.19.009027.

[25] P. C. Beard, F. Perennes, and T. N. Mills, "Transduction mechanisms of the Fabry-Perot polymer film sensing concept for wideband ultrasound detection," *IEEE Trans. Ultrason. Ferroelectr. Freq. Control*, vol. 46, no. 6, pp. 1575–1582, Jan. 1999. DOI: 10.1109/58.808883.

[26] M. Z. Cheng and Y. Z. Chao, "Sensitive label-free and compact ultrasonic sensor based on double silicon-on-insulator slot micro-ring resonators," *Optik*, vol. 178, pp. 1029–1034, Jan. 2019. DOI: 10.1016/j.ijleo.2018.09.101.